

Steplike Behavior in Grain-Size-Dependent Optical Emission of Plasma Induced by Laser-Ablating Granular Material

Xiao-long Li (李小龙)^{1,2,†} Ya-ju Li (李亚举)^{1,2,‡} Song-ting Li (李松庭),³
 Mao-ji Zhou (周毛吉),^{1,2} Liang-wen Chen (陈良文),^{1,2} Ju Meng (孟举),⁴
 Dong-bin Qian (钱东斌)^{1,2,*} Jie Yang (杨杰),^{1,2} Shao-feng Zhang (张少峰),^{1,2} Yong Wu (吴勇),⁴
 and Xin-wen Ma (马新文)^{1,2,†}

¹ Institute of Modern Physics, Chinese Academy of Sciences, Lanzhou 730000, China

² University of Chinese Academy of Sciences, Beijing 100049, China

³ Institute of Photonics & Photon-Technology, Northwest University, Xi'an 710069, China

⁴ Institute of Applied Physics and Computational Mathematics, Beijing 100000, China

(Received 7 January 2021; revised 5 July 2021; accepted 29 July 2021; published 10 August 2021)

Optical emission of plasma induced by a pulsed laser ablating the surface of a randomly packed granular (RPG) material in air is investigated experimentally, taking sieved copper microspheres with discrete diameters, d , ranging from 49 to 390 μm as examples. We find a steplike phenomenon (also called a critical-like phenomenon) in the dependence of plasma emission on the grain size: when d is less than a critical size, only weak emissions are detected; however, when d exceeds the critical size, the emissions abruptly become at least 5 times stronger. Such a phenomenon can be explained by considering the RPG material as a non-Newtonian fluid with a yield stress and an effective viscosity. Specifically, in the range of the grain size above (below) the critical value, the RPG target has a yield stress larger (smaller) than the shock pressure imparted by the energetic processes of plasma generation and expansion, and thus, behaves like an elastic solid (a viscous fluid) to assist (impede) the formation of the plasma with high temperature and high density as an optical emission source for spectrochemical analysis. This work not only has significance in assessing a lower size limit for direct multielement analysis of RPG material using laser-induced breakdown spectroscopy (LIBS), but also shows that the mechanical characteristics of RPG material may be probed using LIBS.

DOI: 10.1103/PhysRevApplied.16.024017

I. INTRODUCTION

Since the pioneering work of Wisbrun *et al.* in the 1990s [1], laser-induced breakdown spectroscopy (LIBS) has been widely accepted as a promising technique for *in situ* multielement analysis of granular materials [2]. With recent increasing interest in randomly packed granular (RPG) materials, which are common in natural and industrial processes, such as soils or sands and metal-nonmetal powders [3–10], researchers have made great efforts to develop the LIBS-based analysis technique. Although its attractive features have been demonstrated, from a practical viewpoint, in contrast to the case of hard block materials, the plasma formed from a RPG surface is usually far from the ideal case as an optical emission source for spectrochemical analysis. This is because as a kind of typical soft matter, a RPG material generally absorbs a certain portion of energy and particles belonging to the plasma

during its generation and expansion, initiating a cratering process [11] and resulting in significant degradation of the quality of LIBS signals [12].

Up to now, many efforts have been dedicated to the improvement of the LIBS signal quality of a soft sample under the requirement of minimal or even no sample preparation. Kagawa and co-workers [13,14] reported a breakthrough study on LIBS of silicon grease by putting it onto a metal plate as a subtarget. It is demonstrated that the subtarget compensates for the absence of a hard surface in the soft-matter case and assists plasma formation to a level adequate for analysis purposes. Thereafter, the approach has been expanded to various RPG samples by putting them on hard subtargets or into small holes [9,15–22]. Although this approach is more convenient than other sample preparations, such as RPG samples pressed into pellets [23], it is not appropriate for many *in situ* applications, especially those in challenging environments, where no form of sample preparation is allowed.

Actually, in studies on LIBS of RPG samples and related applications, the main purpose of sample preparation is to give the sample solidlike mechanical characteristics.

*qiandb@impcas.ac.cn

†x.ma@impcas.ac.cn

‡Xiao-long-Li and Ya-ju Li contributed equally to this work.

Therefore, the prerequisite for completely eliminating preparation procedures is that the RPG sample itself can exhibit “good” mechanical performance to support the shock pressure imparted by energetic processes of plasma generation and expansion (hereinafter called laser-induced shock pressure), reducing, as far as possible, the efficiency of absorption of energy and particles belonging to the plasma. For one type of RPG sample with a given grain packing mode, size distribution, roughness, and shape, grain size is the most important factor that influences its mechanical characteristics (usually smaller sizes lead to poorer mechanical characteristics) [24]. Recent works have frequently demonstrated that the LIBS signal can be used for the estimation of a sample’s mechanical characteristics, more specifically, the estimation of sample hardness [25–27]. Thus, a study on size-dependent LIBS for a given type of RPG sample over a wide size range is essential for understanding the mechanical performance of RPG material to support such a laser-induced shock pressure. Furthermore, it is expected to provide useful information for assessing the feasibility of direct LIBS-based analyses of RPG materials. However, no studies have been carried out to tackle the issue.

Here, taking randomly packed copper micrograins with near-spherical shapes and narrow size distributions as examples, we carry out a specific experiment to measure the dependence of LIBS of a RPG material on the grain size over a range from 49 to 390 μm . We present an observation of a steplike phenomenon (also called critical-like phenomenon) in the variations of the measured plasma emission, temperature, and electron density with the grain size. Combining some photographic measurements on the particle ejecta and the final morphology of the material’s surface after laser ablation, an interpretation for the observed steplike phenomenon will be given by considering the RPG material as a non-Newtonian fluid and introducing one kind of size effect stemming from the mechanical performance of the RPG material to support the laser-induced shock pressure. This study has practical significance in developing the LIBS technique for direct analyses of the elemental composition and mechanical characteristics of RPG materials.

II. EXPERIMENTAL SYSTEM

The copper (Cu) material used in this study comes from a commercial source, which consists of polydisperse micrograins (density, 8.9 g/cm³) synthesized through a hydrothermal method. These polydisperse micrograins are sieved using stainless-steel wire sieves to prepare nine size-selected granular samples. The grain shape and size distribution are measured by scanning electron microscopy (SEM, FEI Nano450, see Fig. 1), showing that the nine samples (labeled S_n , $n = 1\text{--}9$) have a near-spherical shape and a narrow distribution around the central diameter

at 390 (360–430), 297 (277–317), 218 (203–233), 132 (122–142), 109 (104–114), 95 (90–100), 77 (72–83), 69 (64–74), and 49 (44–54) μm . Each sample fills the same cubic container (10-cm side length) to brim and each sample surface is leveled using a straight edge without any shaking or noticeable compaction, thus producing nine loosely RPG samples with fairly flat surfaces. By measuring the mass of grains in the container and the volume of the container, we determine the packing fractions to be between 0.56 and 0.59, depending on the grain size.

The experimental arrangement of beam optics, target, and diagnostics is shown schematically in Fig. 2. A 1064-nm *Q*-switched Nd:YAG laser, operating with 7-ns pulse width and 1-Hz pulse repetition rate, is used as the ablation source. The laser beam is focused using quartz of 80-mm focal length lens (labeled as lens 1). Each sample is exposed to air at atmospheric pressure. The lens-to-sample distance is set 68 mm, i.e., the sample surface is positioned off the focal plane by a distance of 12 mm closer to lens 1. The laser spot size on the sample surfaces is estimated by a standard knife-edge method to be about 600 μm , which is sufficiently large compared with the grain sizes used here. Such an arrangement for the lens-to-sample distance is beneficial for reproducible breakdown and plasma plume for each sample. The laser-pulse energy at the sample surface is measured by using an energy meter and set at 60, 80, and 100 mJ, thus corresponding to a laser intensity range of $(3\text{--}5) \times 10^9 \text{ W/cm}^2$. A dichroscope (Thorlabs, DMLP 900) is used to transmit the laser beam and to reflect the plasma emission light. The emission light is collected by a lens system and a quartz fiber that is coupled to an Echelle spectrograph (LTB, ARYELLE 200) with an intensified CCD (ICCD, Andor, DH 334 T) camera. To ensure meaningful calculations of the spatially integrated plasma parameters, optical emission spectra are recorded by employing a delay time of 1 μs to the laser pulse and a gate width of 2 μs . Besides the indispensable spectroscopic diagnosis, additional photographic diagnoses are used in the present experiment, including a high-spend camera (Phantom, V2012) to record the image sequences of particle ejecta after laser ablation from a side-view perspective at a frame rate of 100 000 frames/s, and a handheld blue-laser three-dimensional (3D) scanner (Shanghai Digital Manufacturing Co., Ltd) to record the morphology of the final surface after laser ablation using a resolution of around 100 μm .

During the experiment, the sample container is moved on the plane perpendicular to the laser beam using a two-dimensional (2D) mobile platform. To provide a fresh point for each laser shot, we use two special operations: (i) the sample is moved fast enough to avoid the laser shot hitting the granular craters induced by previous laser pulses; and (ii) the sample in the container is emptied, refilled, and leveled in the same way after every 60 single-shot measurements. The entire duration of the cratering process

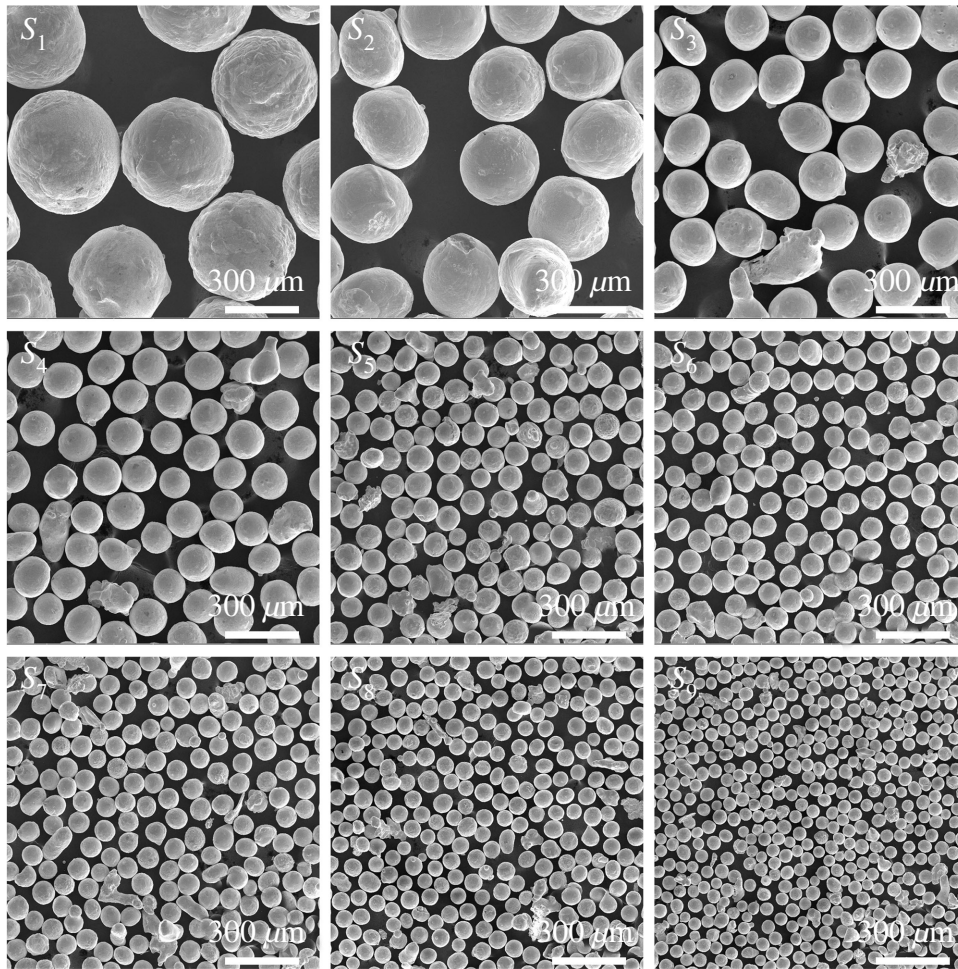


FIG. 1. SEM images of sieved Cu grains used in this study. Scale is given in the frames.

involved here is in the order of 100 ms. A laser working in low-repetition-rate (1 Hz) mode ensures that plasma formation and spectroscopic measurements of subsequent laser pulses are almost not disturbed by granular ejecta induced by previous laser pulses.

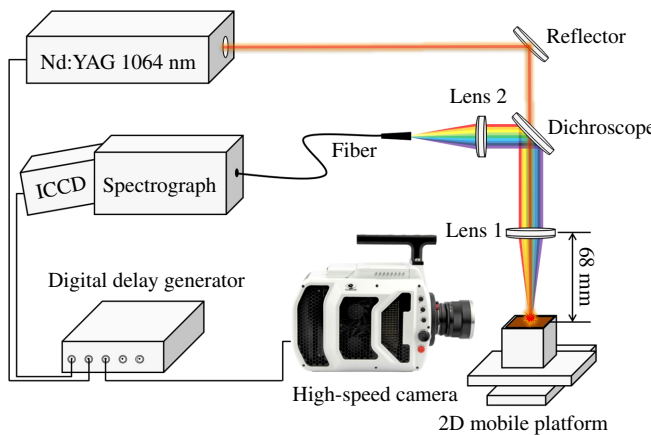


FIG. 2. Schematic diagram of the experimental arrangement.

III. SPECTROSCOPIC RESULTS

We select the three lines of CuI at 510.55, 515.32, and 521.82 nm, which have been frequently used in previous LIBS studies [28–30], for plasma diagnostics. Taking the plasma emissions induced by the 80-mJ laser pulse as examples, in the left part of Fig. 3, we present the emission spectra (average of 60 single-shot measurements) over the wavelength range from 508 to 524 nm for the nine samples. One can see two distinct regions of the emission-intensity distributions. The plasma emissions are weak for samples with grain sizes below about 100 μm ; however, above the size value, an abrupt enhancement of the plasma emission is observed. The features of the emission-intensity distributions with the grain size for 60- and 100-mJ laser pulses are very similar to the 80-mJ case, and thus, are not shown here.

To present the grain-size dependence of the plasma emission more clearly, in Fig. 4, we plot the emission intensities versus the grain diameter for the three selected lines. The intensity of each line is obtained by integrating the corresponding peak area in each spectrum averaged over 60 single-shot measurements. The error bars are determined by calculating the standard deviations from 10

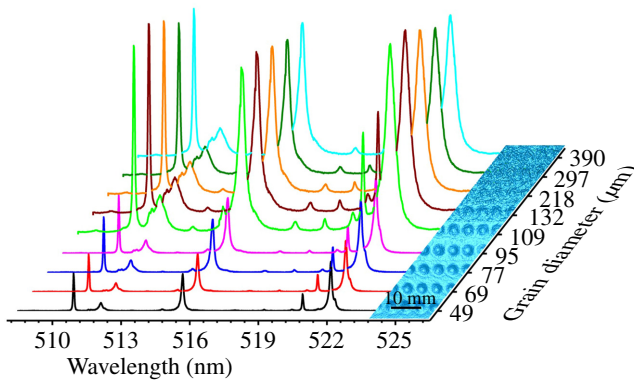


FIG. 3. LIBS spectra of nine loosely RPG samples induced by 80-mJ laser pulse (left) and corresponding final surface morphologies after laser ablation (right; scale is given in the frame).

replicate spectra. It is clearly observed that there is a step-like behavior in the variation of the emission intensity with grain size (d) for each line. Specifically, when d is less than a critical value, d_c , the intensity of each line is very weak and significantly depends on the grain size; however, when d exceeds the critical value, each line intensity abruptly becomes at least 5 times stronger and only shows a mild dependence on the grain size. For 80- and 100-mJ laser pulses, the intensities of the three lines in the $d > d_c$ region are even 1 or 2 orders of magnitude larger than those in the $d < d_c$ region. The specific d_c value involved here should be located in a narrow region between 95 and 135 μm.

Plasma temperature and electron density are the two most important plasma parameters because many other parameters can be expressed as the functions of these two parameters. Here, following previous studies [31,32],

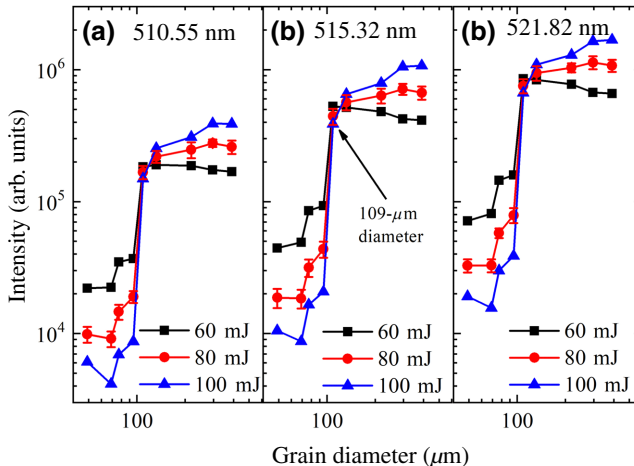


FIG. 4. Emission intensities of CuI lines at 510.55, 515.32, and 521.82 nm as a function of grain diameter at different laser-pulse energies.

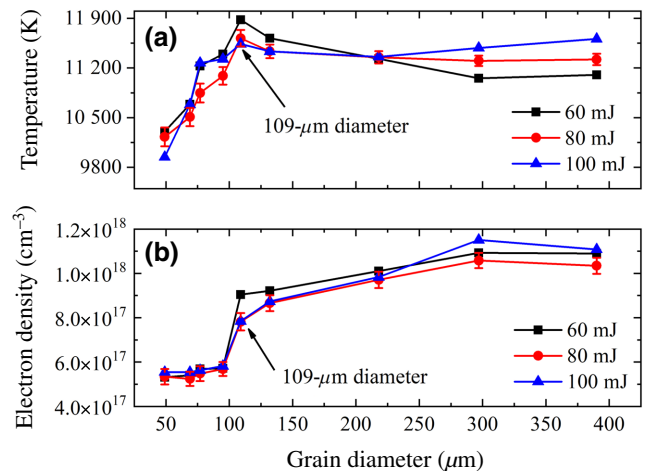


FIG. 5. Plasma temperature (a) and electron density (b) as a function of grain diameter at different laser-pulse energies.

the electron density is calculated by analyzing the Stark-broadened profile of the CuI line at 510.55 nm with a Lorentzian fit. The plasma temperature can be determined, in the framework of the local-thermal-equilibrium (LTE) approximation, using the Boltzmann plot method. In this study, we use the CuI lines at 510.55, 515.32, and 521.82 nm to calculate the plasma temperature. These lines are used because their atomic data are easily available from the literature [33,34], their emission intensities are always quite detectable, and self-absorptions are negligible under the present experimental conditions. The calculated values of plasma temperature and electron density are plotted in Fig. 5. One can see that, for the three laser energies, the plasma temperature and electron density with incremental grain size exhibit similar steplike behavior to that shown in the emission intensities of the CuI lines measured. It is noted that the variations of temperature and electron density near the critical size are not as steep as the measured emission intensities.

In a laser-induced plasma, directly influencing the emission intensity of a spectral line is the number density of the emitting species and the plasma temperature, since the line intensity is usually simulated under the LTE approximation using the following relation [22]:

$$I_{ij} \propto N e^{(-E_j/k_B T)} / U(T). \quad (1)$$

Here, E_j is the energy of the upper level related to the spectral line, k_B is the Boltzmann constant, T is the plasma temperature, N is the number density of the emitting species, and $U(T)$ is the partition function of the emitting species. Therefore, variations of the number density of Cu atoms with grain size can be derived by putting the corresponding values of the measured line intensity and calculated plasma temperature into Eq. (1). Here, we use the specific line of CuI at 510.55 nm to derive the dependence

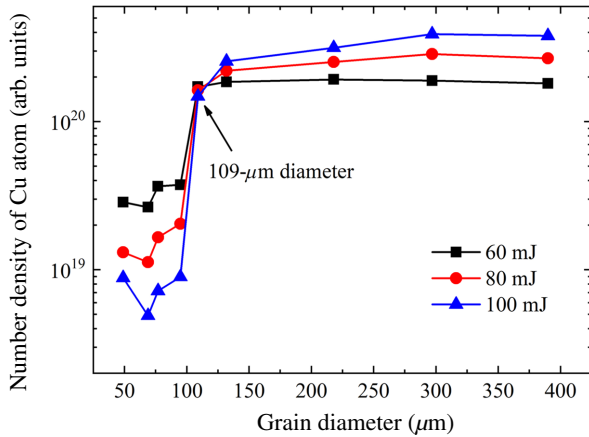


FIG. 6. Relative number density of Cu atoms as a function of grain diameter at different laser-pulse energies.

of the relative number density of Cu atoms on grain size. The atomic level data for the calculation of the partition function of a neutral Cu atom are retrieved from the NIST atomic level database. The derived results are shown in Fig. 6. It can be clearly seen that the variations of the relative number density of Cu atoms with grain size are almost the same as the line intensities measured, which implies that, for the current experiment, the number density of Cu atoms plays a more key role in influencing the observed grain-size-dependent plasma-emission features compared with the plasma temperature.

IV. EXPLANATION AND DISCUSSION OF SPECTROSCOPIC RESULTS

Considering that the disturbances to the plasma formation and the spectroscopic measurement among laser pulses have been effectively avoided in current experiment, the only implication from such a steplike phenomenon shown in Figs. 4–6 is that certain grain-size-dependent changes to the physical properties of the RPG samples occur, resulting in quite different circumstances for plasma formation in the two size regions below and above the critical size. According to the fundamentals of laser-matter interaction [35–37], what we can summarize is that four physical properties of a given type of RPG material may have a significant influence on plasma formation: (i) morphological, such as surface roughness; (ii) thermal, such as thermal conductivity; (iii) optical, such as scattering coefficient; and (iv) mechanical, such as hardness. Previous experimental studies [38] have demonstrated that, for a RPG sample with a smaller grain size, the first two properties lead to a higher vaporization efficiency in laser ablation, and thus, to the formation of a “higher-temperature and higher-density” plasma. This implies that they are impossible to use to explain the steplike phenomenon observed. For the third property, it is totally out

of the question because the grain sizes involved here are far larger than the laser wavelength, indicating negligible differences in scattering efficiency among the samples [6]. Therefore, we deduce that the fourth property plays a crucial role in understanding such a phenomenon observed. The deduction is also based on two mechanical fundamentals of a granular material [24]. One is that the RPG material is a complex nonlinear mechanical system and often varies dramatically between solidlike and fluidlike, depending on external circumstances. Another is that the mechanical performance of the RPG material to support a fixed external pressure depends on grain size: usually smaller sizes lead to poorer mechanical performances.

The complex physical processes in the generation and expansion of plasma induced by a moderate-energy laser beam interacting with metallic targets were reported in detail by Beilis [37]. A series of works by Kagawa and co-workers [39–41] pointed out that the development of laser plasma produced in a surrounding gas can be simplified into two distinct stages. In the first stage, the plasma is called a primary plasma, which acts as an initial explosion-energy source to generate a shock wave. At moderate-laser-power-density ablations, like the present cases, the shock wave begins to heat the air enough to produce a laser-supported absorption wave (LSAW). In the second stage, the plasma expands with time around the primary one and is heated by the LSAW, which emits sharp spectral lines used for elemental analysis. The most important point in the formation of the secondary plasma is that its formation energy is mainly supplied by the total kinetic energy of the particles gushing from the primary plasma. Certainly, the absorption of laser radiation by primary plasma, which includes the plasma plume and shocked background gas, also contributes the formation energy. During the formation of the secondary plasma, if certain portions of the LSAW energy and gushed particles impacting on the sample surface are absorbed due to the poor mechanical performance for supporting the laser-induced shock pressure, the formation energy will depend on the mechanical performance of the sample; poorer mechanical performances to higher absorption efficiencies, and thus, to lower formation energies.

Coming back now to the spectroscopic results obtained by us, higher (lower) plasma temperatures and number densities of electrons and Cu atoms when $d > d_c$ ($d < d_c$) indicates that a secondary plasma with high temperature and high density is (not) well generated in the size region. To explain the results, we consider the RPG material as a non-Newtonian Bingham fluid, building on previous studies [42], that is, a fluid with a yield stress and an effective viscosity. Our results imply that, in the $d > d_c$ region, the sample has a yield stress larger than the laser-induced shock pressure, and thus, behaves like an elastic solid. The LSAW energy and the particles (including electrons and Cu atoms) gushing from the primary plasma cannot be

absorbed efficiently by the RPG sample, favoring the formation of a high-temperature and high-density secondary plasma. Following this line, in the $d < d_c$ region, the sample has a yield stress smaller than the laser-induced shock pressure, and thus, behaves like a fluid. In contrast to the case of $d > d_c$, the shock pressure initiates efficient absorption of the LSAW energy and particles gushing from the primary plasma, to provide the energy required for sample deformation, thus impeding the formation of a high-temperature and high-density secondary plasma. The absorption efficiency depends on the sample's mechanical performance, where the mechanical performance should have a positive correlation with the effective viscosity (the resistance to flow). For a RPG material with a higher fluidity (or a lower viscosity), it would be expected to have a higher absorption efficiency. In the $d < d_c$ region, the plasma temperature obtained by us (see Fig. 5) seems to imply a negative correlation between the fluidity and grain size under the current experimental conditions.

To provide further evidence for the above interpretation, the final surface morphologies of the nine samples after laser ablation with 80-mJ pulse energy are recorded using a handheld blue-laser 3D scanner and are shown in the right part of Fig. 3. One can see that, in the size range of 49 to 109 μm , single-shot ablations create clean-cut granular craters of a few millimeters in diameter; however, in the size range of 135 to 390 μm , clean-cut craters cannot be well created any more. The presence (absence) of a clean-cut crater indicates that the samples exhibit a poor (good) mechanical performance to support the laser-induced shock pressure, initiating (impeding) efficient absorption for the LSAW energy and gushed particles to provide the energy required for sample deformation. Furthermore, two representative movies are also recorded using a high-spend camera and presented in image sequence format in Fig. 7, which show the plasma evolution and subsequent cratering process for the cases of the smallest and largest grains used in this study (see Movies M1 and M2 within the Supplemental Material [43]). In Fig. 7, time t corresponds to a specific delay time with respect to the laser pulse. Plasma evolution after laser ablation is depicted by the saturated region on the target surface (bright spot in images of $t = 0.01\text{--}0.08$ ms). One can see that, for the smallest case, a plasma with weaker emission and a shorter lifetime is produced, implying that the laser-induced shock pressure initiates efficient absorption of energy and particles belonging to the plasma, to provide considerable energy for sample deformation. Indeed, a fluent cratering process is directly indicated in the subsequent images of $t = 1\text{--}10$ ms by an ejecta curtain, which propagates radially away from the laser spot (Movie M1 within the Supplemental Material [43]). However, for the largest case, a plasma with stronger emission and a longer lifetime is produced and only several grains near the surface are ejected (Movie M2 within the Supplemental

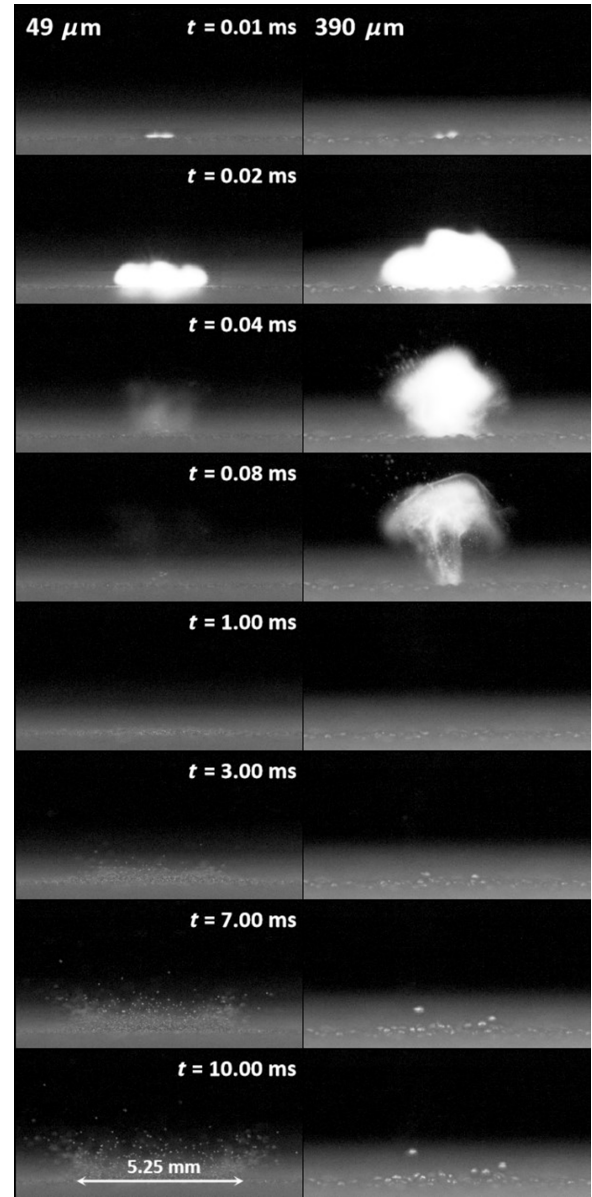


FIG. 7. Image sequence showing the plasma evolution and cratering process after laser ablation for the smallest (left column) and largest (right column) grains used in this study. Scale is given in the frame.

Material [43]), providing visual evidence that the sample has a yield stress larger than the laser-induced shock pressure, and thus, behaves like an elastic solid, to prevent efficient energy absorption and sample deformation.

Now let's consider the reason why the variations in plasma temperature and electron density with the grain size are not as steep as that of the number density of Cu atoms near the critical size. First, using the FLYCHK tool [44], we estimate the LTE ratio of the Cu^{2+} state to the Cu^+ state based on the Saha-Boltzmann equation with the values of temperature and electron density shown in Fig. 5 and

find that the ratios are always less than 0.01, implying that, if there are no additional electron-compensation channels, the electrons come almost entirely from the single ionization of Cu atoms. If these are the electrons involved in our experiment, variations in the electron density with grain size should be very close to the cases of the number density of Cu atoms because similar portions of electrons and Cu atoms impact on the sample surface and are then absorbed. Obviously, the supposition is untenable. A specific feature of pulsed-laser interaction with metallic targets over a range of laser power density like that of the current experiment is that the pulse duration is significantly longer than the initiation time of the primary plasma [37]. The expanding plume of the primary plasma and the shocked air can thus absorb energy from the incoming laser pulse, leading to laser shielding. This may indicate that the heated air atoms indisputably contribute to the electron density and compensate for the temperature in some way. However, the situation of the number density of Cu atoms is completely different from that of the electron density and plasma temperature. The “poor” mechanical performance of the sample leads to direct loss of Cu atoms gushing from the primary plasma without any follow-up compensation channel.

In addition, for the set of loosely RPG Cu samples used here, the yield stress depends on both the packing fraction and the grain size. It is natural to ask if the steplike phenomenon observed is a manifestation of the critical packing state, as reported by Umbanhowar and Goldman [45]. We show that this cannot be the case, as follows. An additional set of RPG Cu samples is prepared in the same way, except for shaking the samples sufficiently for there to be no further reduction in volume. For the sake of comparison between the two sets of RPG samples, the trends of the packing fraction and the emission intensity (taking the 510.55-nm line induced by the 60-mJ laser pulse as an example) versus the grain diameter are presented in Fig. 8. One can see that, although the packing fraction in the tightly packed state has a systematic increase by at least 3.5% for each grain size, the corresponding steplike phenomenon in the size-dependent optical emission occurs at the same critical size with the loosely packed state. This implies that the grain size may be the most important determinant of the yield stress of the samples involved here, and thus, plays a key role in dominating the occurrence of the steplike phenomenon.

This steplike phenomenon should be a common phenomenon in LIBS of RPG materials. Knowledge of such a phenomenon is very useful for developing a modern technique for direct multielement analysis of RPG material using LIBS. The most difficult problem with the analytical technique is that the expected linear relationship between the emission intensity and corresponding element concentration is often flawed due to the irreproducibility of the plasma produced from the RPG surface with different grain

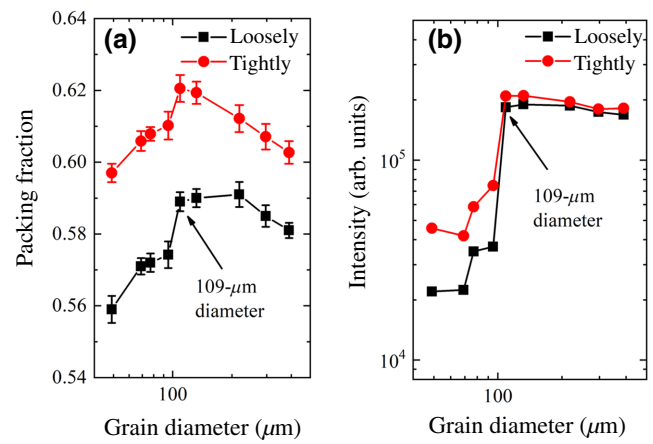


FIG. 8. Comparison between loosely and tightly RPG samples. (a) Packing fractions as a function grain diameter. (b) Emission intensities of the 510.55-nm line induced by the 60-mJ laser pulse as a function of grain diameter.

sizes. The steplike phenomenon tell us that this problem can be controlled in a relatively gentle state once the grain size is beyond the critical value. In other words, there is a well-defined grain size above which the RPG material exhibits favorable mechanical characteristics for LIBS-based analysis purposes, indicating that any sample preparation may become unnecessary. This is very important for related applications in hostile and inaccessible environments, such as radiation hazards [5] and space exploration [46–48]. In addition, as mentioned above, when the grain size is below the critical value, the relationship between the plasma temperature and grain size (see Fig. 4) seems to provide information on the size-dependent granular fluidity (or effective viscosity) of the RPG sample. No work has been reported on the analysis of the mechanical properties of RPG material using LIBS. We believe that this is of considerable interest for future works. On the other hand, considering that the yield stress of the RPG material is the decisive factor for the steplike phenomenon, the specific value of critical size should depend on many granular parameters, such as roughness and shape. Further works are still needed for a better understanding of the role of each parameter in such a steplike phenomenon.

V. CONCLUSIONS

We investigate the grain-size dependence of the optical emissions of plasmas induced by laser-ablating RPG copper samples in the size range of 49 to 390 μm. We find that the optical emission, excitation temperature, and number densities of electrons and Cu atoms in the plasma show a steplike phenomenon (also called the critical-like phenomenon) with increasing grain size, d . Combining photographic measurements of the image sequences of particle ejecta and the final surface morphologies after laser ablation, we demonstrate that the specific grain size related

to the occurrence of such a steplike phenomenon represents a threshold, above (below) which the RPG sample has a yield stress larger (smaller) than the shock pressure imparted by the energetic process of plasma generation and expansion, and thus, behaves like an elastic solid (a viscous fluid) to assist (impede) the formation of plasma with high temperature and high density as an optical emission source for spectrochemical analysis. The present results not only have potential use in the assessment of a lower size limit for performing direct multielement analysis of RPG materials using LIBS, but also provide a possible avenue to probe the mechanical characteristics of RPG materials using LIBS.

ACKNOWLEDGMENTS

The authors are grateful to Jin Yu (Shanghai Jiao Tong University, China) for many scientific discussions and advice. This research is supported, in part, by the National Key R&D Program (Grant No. 2017YFA0402300) and the NSFC program (Grants No. 11974359 and No. U1632143).

- [1] R. Wisbrun, I. Schechter, R. Niessner, H. Schriider, and K. L. Kompa, Detector for trace elemental analysis of solid environmental samples by laser plasma spectroscopy, *Anal. Chem.* **66**, 2964 (1994).
- [2] J. P. Singh and S. N. Thakur, *Laser-induced Breakdown Spectroscopy* (Elsevier, Amsterdam, The Netherlands, 2007).
- [3] R. Viskup, B. Praher, T. Stehrer, J. Jasik, H. Wolfmeir, E. Arenholz, J. D. Pedarnig, and J. Heitz, Plasma plume photography and spectroscopy of Fe-Oxide materials, *Appl. Surf. Sci.* **255**, 5215 (2009).
- [4] T. Stehrer, B. Praher, R. Viskup, J. Jasik, H. Wolfmeir, E. Arenholz, J. Heitzab, and J. D. Pedarnig, Laser-induced breakdown spectroscopy of iron oxide powder, *J. Anal. At. Spectrom.* **24**, 973 (2009).
- [5] E. J. Judge, J. E. Barefield, J. M. Berg, S. M. Clegg, G. J. Havrilla, V. M. Montoya, L. A. Le, N. Leon, and L. N. Lopez, Laser-induced breakdown spectroscopy measurements of uranium and thorium powders and uranium ore, *Spectrochim. Acta Part B: Atom. Spectrosc.* **83**, 28 (2013).
- [6] S. J. Pandey, R. Locke, R. M. Gaume, and M. Baudelet, Effect of powder compact density on the LIBS analysis of Ni impurities in alumina powders, *Spectrochim. Acta Part B: Atom. Spectrosc.* **148**, 99 (2018).
- [7] L. Xu, V. Bulatov, V. V. Gridin, and I. Schechter, Absolute analysis of particulate materials by laser-induced breakdown spectroscopy, *Anal. Chem.* **69**, 2103 (1997).
- [8] B. Sallé, D. A. Cremers, S. Maurice, and R. C. Wiens, Laser-induced breakdown spectroscopy for space exploration applications: Influence of the ambient pressure on the calibration curves prepared from soil and clay samples, *Spectrochim. Acta Part B: Atom. Spectrosc.* **60**, 479 (2005).
- [9] N. Idris, K. Kagawa, F. Sakan, K. Tsuyuki, and S. Miura, Analysis of heavy metal pollution in soil using transversely excited atmospheric CO₂ laser-induced plasma by trapping the soil in microstructured holes on metal subtargets, *Appl. Spectrosc.* **61**, 1344 (2007).
- [10] R. X. Yi, J. M. Li, X. Y. Yang, R. Zhou, H. W. Yu, Z. Q. Hao, L. B. Guo, X. Y. Li, X. Y. Zeng, and Y. F. Lu, Spectral interference elimination in soil analysis using laser-induced breakdown spectroscopy assisted by laser-induced fluorescence, *Anal. Chem.* **89**, 2334 (2017).
- [11] J. O. Marston and F. Pacheco-Vázquez, Millimetric granular craters from pulsed laser ablation, *Phys. Rev. E* **99**, 030901(R) (2019).
- [12] H. Kurniawan, S. Nakajima, J. E. Batubara, M. Marpaung, M. Okamoto, and K. Kagawa, Laser-induced shock wave plasma in glass and its application to elemental analysis, *Appl. Spectrosc.* **49**, 1067 (1995).
- [13] M. M. Suliyanti, R. Hedwig, H. Kurniawan, and K. Kagawa, The role of sub-target in the transversely excited atmospheric pressure CO₂ laser-induced shock-wave plasma, *Jpn. J. Appl. Phys.* **37**, 6628 (1998).
- [14] K. Kagawa, T. J. Lie, R. Hedwig, S. N. Adulmajid, M. M. Suliyanti, and H. Kurniawan, Subtarget effect on laser plasma generated by transversely excited atmospheric CO₂ laser at atmospheric gas pressure, *Jpn. J. Appl. Phys.* **39**, 2643 (2000).
- [15] H. Oki, H. Suyanto, K. H. Kurniawan, T. J. Lie, Y. I. Lee, F. Sakan, N. Idris, and K. Kagawa, Water analysis by laser-induced shock wave plasma spectroscopy using recrystallized KBr powder confined in a cylindrical tube, *Jpn. J. Appl. Phys.* **43**, 1036 (2004).
- [16] M. Pouzar, T. Kratochvil, L. Capek, L. Smolakova, T. Cernohorsky, A. Krejcová, and L. Hromadko, Quantitative LIBS analysis of vanadium in samples of hexagonal mesoporous silica catalysts, *Talanta* **83**, 1659 (2011).
- [17] A. Khumaeni, H. Niki, K. Fukumoto, Y. Deguchi, K. Kurihara, K. Kagawa, and Y. I. Lee, A unique technique of laser-induced breakdown spectroscopy using transversely excited atmospheric CO₂ laser for the sensitive analysis of powder samples, *Curr. Appl. Phys.* **11**, 423 (2011).
- [18] A. Khumaeni, Z. S. Lie, H. Niki, K. H. Kurniawan, E. Tjoeng, Y. I. Lee, K. Kurihara, Y. Deguchi, and K. Kagawa, Direct analysis of powder samples using transversely excited atmospheric CO₂ laser-induced gas plasma at 1 atm, *Anal. Bioanal. Chem.* **400**, 3279 (2011).
- [19] J. Iqbal, M. Pardede, E. Jobilong, R. Hedwig, M. Ramli, A. Khumaenie, W. S. Budi, N. Idris, S. N. Abdulmadjid, K. Lahna, M. A. Marpaung, I. Karnadi, Z. S. Lie, H. Suyanto, D. P. Kurniawan, T. J. Lie, K. H. Kurniawan, K. Kagawa, and M. O. Tjia, Shock wave plasma generation in low pressure ambient gas from powder sample using subtarget supported micro mesh as a sample holder and its potential applications for sensitive analysis of powder samples, *Microchem. J.* **142**, 108 (2018).
- [20] A. Khumaeni, M. Ramli, Y. Deguchi, Y. I. Lee, N. Idris, K. H. Kurniawan, T. J. Lie, and K. Kagawa, New technique for the direct analysis of food powders confined in a small hole using transversely excited atmospheric CO₂ laser-induced gas plasma, *Appl. Spectrosc.* **62**, 1344 (2008).
- [21] Z. S. Lie, M. Pardede, R. Hedwig, M. M. Suliyanti, K. H. Kurniawan, Y. I. Lee, K. Kagawa, I. Hattori, and

- M. O. Tjia, Spectrochemical analysis of powder using 355 nm Nd-YAG laser-induced low-pressure plasma, *Anal. Bioanal. Chem.* **390**, 1781 (2008).
- [22] Y. Tian, H. C. Cheung, R. Zheng, Q. Ma, Y. Chen, N. Delepine-Gilonc, and J. Yu, Elemental analysis of powders with surface-assisted thin film laser-induced breakdown spectroscopy, *Spectrochim. Acta Part B: Atom. Spectrosc.* **124**, 16 (2016).
- [23] S. C. Jantzi, V. Motto-Ros, F. Trichard, Y. Markushin, N. Melikechi, and A. D. Giacomo, Sample treatment and preparation for laser-induced breakdown spectroscopy, *Spectrochim. Acta Part B: Atom. Spectrosc.* **115**, 52 (2016).
- [24] J. Duran, *Sands, Powders, And Grains: An Introduction to the Physics of Granular Materials* (Springer, New York, 2000).
- [25] S. N. Abdulmadjid, M. Pardede, H. Suyanto, M. Ramli, K. Lahna, A. M. Marpaung, R. Hedwig, Z. S. Lie, D. P. Kurniawan, K. H. Kurniawan, T. J. Lie, N. Idris, M. O. Tjia, and K. Kagawa, Evidence of feasible hardness test on Mars using ratio of ionic/neutral emission intensities measured with laser-induced breakdown spectroscopy in low pressure CO₂ ambient gas, *J. Appl. Phys.* **119**, 163304 (2016).
- [26] M. Momcilovic, J. Petrovic, J. Ciganovic, I. Cvijovic-Alagic, F. Koldzic, and S. Zivkovic, Laser-induced plasma as a method for the metallic materials hardness estimation: An alternative approach, *Plasma Chem. Plasma Process.* **40**, 499 (2020).
- [27] H. Harse Sattar, H. Ran, W. Ding, M. Imran, M. Amir, and H. Ding, An approach of stand-off measuring hardness of tungsten heavy alloys using LIBS, *Appl. Phys. B* **126**, 5 (2020).
- [28] S. S. Harilal, P. K. Diwakar, and A. Hassanein, Electron-ion relaxation time dependent signal enhancement in ultrafast double-pulse laser-induced breakdown spectroscopy, *Appl. Phys. Lett.* **103**, 041102 (2013).
- [29] M. A. Hafez, M. A. Khedr, F. F. Elaksher, and Y. E. Gamal, Characteristics of Cu plasma produced by a laser interaction with a solid target, *Plasma Sources Sci. Technol.* **12**, 185 (2003).
- [30] A. Fernandez, X. L. Mao, W. T. Chan, M. A. Shannon, and R. E. Russo, Correlation of spectral emission intensity in the inductively coupled plasma and laser-induced plasma during laser ablation of solid samples, *Ana. Chem.* **67**, 2444 (1995).
- [31] D. N. Patel, P. K. Pandey, and R. K. Thareja, Stoichiometric investigations of laser-ablated brass plasma, *Appl. Optics* **51**, B192 (2012).
- [32] Dai Cheng, Haihong Zhu, and Linda Ke, Investigation of plasma spectra during selective laser micro sintering Cu-based metal powder, *Rapid Prototyping J.* **19**, 373 (2013).
- [33] Anmin Chen, Yuanfei Jiang, Tingfeng Wang, Junfeng Shao, and Mingxing Jin, Comparison of plasma temperature and electron density on nanosecond laser ablation of Cu and nano-Cu, *Phys. Plasmas* **22**, 033301 (2015).
- [34] Vassilia Zorba, Xianglei Mao, and Richard E. Russo, Femtosecond laser induced breakdown spectroscopy of Cu at the micron/sub-micron scale, *Spectrochimica Acta Part B* **113**, 37 (2015).
- [35] R. Noll, *Laser-induced Breakdown Spectroscopy* (Springer-Verlog, Berlin, 2012).
- [36] A. W. Miziolek, V. Palleschi, and I. Schechter, *Laser-Induced Breakdown Spectroscopy (LIBS): Fundamentals and Applications* (Cambridge University Press, Cambridge, 2006).
- [37] Isak I. Beilis, Modeling of the plasma produced by moderate energy laser beam interaction with metallic targets: Physics of the phenomena, *Laser Part. Beam.* **30**, 341 (2012).
- [38] L. Y. Yu, J. D. Lu, W. Chen, G. Wu, K. Shen, and W. Feng, Analysis of pulverized coal by laser-induced breakdown spectroscopy, *Plasma Sci. Technol.* **7**, 3041 (2005).
- [39] K. Kagawa, S. Yokoi, and S. Nakajima, Metal plasma induced by the bombardment of 308 nm excimer and 585 nm dye laser pulses at low pressure, *Opt. Commun.* **45**, 261 (1983).
- [40] K. Kagawa, K. Kawai, M. Tani, and T. Kobayashi, XeCl excimer laser-induced shock wave plasma and its application to emission spectrochemical analysis, *Appl. Spectrosc.* **48**, 198 (1994).
- [41] A. M. Marpaung, R. Hedwig, M. Pardede, T. J. Lie, M. O. Tjia, K. Kagawa, and H. Hurniawan, Shock wave plasma induced by TEA CO₂ laser bombardment on glass samples at high pressures, *Spectrochim. Acta Part B: Atom. Spectrosc.* **55**, 1591 (2000).
- [42] J. R. de Bruyn and A. M. Walsh, Penetration of spheres into loose granular media, *Can. J. Phys.* **82**, 439 (2004).
- [43] See the Supplemental Material at <http://link.aps.org/supplemental/10.1103/PhysRevApplied.16.024017> for details of the plasma evolution and subsequent cratering process and movies M1 and M2, corresponding to the smallest and largest grains used in this study, respectively.
- [44] H.-K. Chung, M. H. Chen, W. L. Morgan, Y. Ralchenko, and R. W. Lee, FLYCHK: Generalized population kinetics and spectral model for rapid spectroscopic analysis for all elements, *High Energy Density Physics* **1**, 3 (2005).
- [45] P. Umbanhowar and D. I. Goldman, Granular impact and the critical packing state, *Phys. Rev. E* **82**, 010301(R) (2010).
- [46] R. C. Wiens, S. Maurice, B. Barraclough, M. Saccoccia, W. C. Barkley, J. F. Bell, et al., The ChemCam instrument suite on the Mars science laboratory (MSL) rover: Body unit and combined system tests, *Space Sci. Rev.* **170**, 167 (2012).
- [47] R. C. Wiens, S. Maurice, and F. Rull Perez, The SuperCam remote sensing instrument suite for the Mars 2020 rover mission: A preview, *Spectroscopy* **32**, 50 (2017).
- [48] F. Rivera-Hernandez, D. Y. Sumner, N. Mangold, K. M. Stack, O. Forni, H. Newsom, A. Williams, M. Nachon, J. L'Haridon, O. Gasnault, R. Wiens, and S. Maurice, Using ChemCam LIBS data to constrain grain size in rocks on Mars: Proof of concept and application to rocks at Yellowknife Bay and Pahrump Hills, Gale crater, *Icarus* **321**, 82 (2019).